J. Appl. Comput. Mech., 8(3) (2022) 1043-1053
DOI: 10.22055/jacm.2022.38275.3189

ISSN: 2383-4536
jacm.scu.ac.ir

Shahid Chamran University of Ahvaz

Journal of Applied and Computational Mechanics

Research Paper

A Kinetic Flux-vector Splitting Scheme for Two-layer Shallow Flow Model

Saqib Zia[1], Saeed Ullah Khan[2], Omar Rabbani[3], Munshoor Ahmed[4], Asad Rehman[5]

[1] Department of Mathematics, COMSATS University Islamabad, Park Road, Chak Shahzad Islamabad, Pakistan, Email: saqibzia81@hotmail.com

[2] School of Mathematics and Statistics, Zhengzhou University, Zhengzhou 450001, China, Email: saeedkhan.u@gmail.com

[3] Department of Mathematics, COMSATS University Islamabad, Park Road, Chak Shahzad Islamabad, Pakistan, Email: mathematixian@gmail.com

[4] Department of Mathematics, COMSATS University Islamabad, Park Road, Chak Shahzad Islamabad, Pakistan, Email: manshoor@comsats.edu.pk

[5] Department of Mathematics, University of Education, Lahore, Pakistan, Email: assad013@gmail.com

Received August 05 2021; Revised February 09 2022; Accepted for publication February 09 2022.
Corresponding author: S. Zia (saqibzia81@hotmail.com)

Abstract. In this article, two-layer shallow flow model with non-flat basal topography is considered. The presence of coupling terms in two layers make the system conditional hyperbolic. The kinetic flux-vector splitting (KFVS) scheme is applied to approximate the corresponding one-dimensional two-layer shallow flow equations. Our interest lies in the numerical approximation of the model referred to above, the complexity of which poses numerical problems. The higher order accuracy of the scheme is achieved by using a MUSCL-type initial reconstruction and Runge-Kutta time stepping method. The scheme is able to treat variety of flow conditions. A number of test cases are carried out to verify the performance of the suggested method. The conservation and solution element (CESE) scheme is used for comparison. It is observed from the comparison that KFVS resolves the shocks more effectively than CESE scheme.

Keywords: Two-layer SWEs, KFVS scheme, CESE, non-flat bottom topography, discontinuous solutions, conservation laws.

1. Introduction

The multilayer shallow water equations (SWE's) are commonly used to depict flows with different densities. The variations in density are due to variations in salinity and/or temperature, so this type of layering appear in numerous regular streams, adrift entryways, bays, estuaries and obviously manufactured structures like conduits furthermore, locks etc. A large portion of these streams can be portrayed as shallow, remembering that even a sea may be dealt with as shallow if the profundity is contrasted with the even measurements, particularly when consideration is limited to coastal regions.

Variations in density generally act as a barrier to blending the two superimposed liquids, so it is helpful to investigate the layered flows as the layering has some kind of intrinsic stability. An illustration, which has as of late discovered serious consideration in connected science and numerical investigation, is the superposition of the Mediterranean and the Atlantic in the Strait of Gibraltar [1]. For the modelling of tsunamis generated by underwater landslides, two-layer SWEs can be used see e.g. [2, 3].

The layering is primarily stable, but this stability will be lost under certain conditions, resulting in Kelvin-Helmholtz instability. The layers begin to mix, causing the current flow to change density and discharge as well as to change in type of PDEs. The SWEs are unconditionally hyperbolic in nature, and are relatively simple to investigate numerically. A slight change in the nature of these equations gives additional numerical complexity. It is important to mention that the two-layer SWEs are conditionally hyperbolic. There is a possibility that the system lose hyperbolicity during approximation. Furthermore, with inclusion of non-flat basal topography, some computational challenges are related to this type of mathematical models. For example, well-posedness of the models in appropriate functional spaces and initial data, the balancing of source term with fluxes in the presence of non-smooth basal topography, propagation of discontinuities in solution profile, the proper discretization of source terms in heterogeneous media. Robust, reliable and efficient numerical algorithms are required to address the numerical issues posed by these systems. Numerous authors have discuss about the loss of hyperbolicity in two-layer flows see e.g. [4–10]. Moreover, a lot of researchers have done investigations to mitigate this effect by utilizing physically motivated discharge transfer to stabilize the system [11, 12].

To address some of the above mentioned difficulties, a well-balanced numerical scheme is needed. A well-balanced scheme can effectively handle small perturbations in the steady state solutions. Therefore, these schemes are better suited computing turbulent fluctuations in steady flows, whereas the schemes which are not well-balanced can only handle perturbations at the level of truncation error. A lot of work about well-balanced schemes to solve depth averaged models have been done in the literature e.g. see [13–18].

Published online: February 20 2022

In the present paper a KFVS scheme [19–22] is applied to solve two-layer shallow flow model. The scheme is a Boltzmann-type and the researchers chose it as it is positivity preserving, robust, efficient and free of Riemann solver property. In [21], the mathematical model was strictly hyperbolic and the authors extended the KFVS to solve it by considering flat bottom topography. This method does have some drawbacks as well i.e. (i) It depends on Maxwellian distribution function, therefore this method is usually complicated due to complexities of the Maxwellian function, thus it is considered to be computationally expensive (ii) It computes the viscous and inviscid fluxes as a single entity. Although this method is computationally expensive yet the scientists prefer it due to its positivity preserving property for small values of physical variables.

The KFVS scheme was developed by Deshpande [23] as a result of the kinetic theory based on the fluid-in-class method for classical compressible Euler equations. The Pulline's flux equilibrium method [24] and Rietz's kinetic numerical method [25] are variants of the KFVS scheme. Significant improvements were made by Partheme [26] who used the characteristic function instead of the Maxwellian distribution function (MDF).

In KFVS, the separation of flux vectors is the method for obtaining up winding bias as a function of numerical flux, which is the obvious consequence if a liquid is treated as a group of particles [19]. Since the motion of the particles is in forward/ backward direction, naturally the fluxes at the cell's interface are also divided into forward/ backward direction, that is,

$$\mathbf{F}_{i+1/2} = \mathbf{F}^{+}(\mathbf{W}_i) + \mathbf{F}^{-}(\mathbf{W}_{i+1}), \tag{1.1}$$

$\mathbf{W}_i$ and $\mathbf{F}(\mathbf{W}_i)$ denote the vectors of conserved quantities and fluxes respectively. Moreover, we extended this scheme to second order and the results of suggested scheme are compared to the CESE scheme [27–29].

The manuscript is arranged as follows. The section 2 presents two-layer SWEs and sections 3 deals with the derivation of 1-D KFVS scheme. The test case studies are incorporated in section 4. In the end conclusions and remarks are given in section 5.

2. Mathematical Model for Two-layer Shallow Water Flow

The one-dimensional two-layer SWEs with bottom topography are given [10] as,

$$\partial_t h_1 + \partial_x(q_1) = 0, \tag{2.1}$$

$$\partial_t q_1 + \partial_x(q_1 u_1 + \frac{g}{2} h_1^2) = -g h_1 \partial_x(h_2 + B(x)), \tag{2.2}$$

$$\partial_t h_2 + \partial_x(q_2) = 0, \tag{2.3}$$

$$\partial_t q_2 + \partial_x(q_2 u_2 + \frac{g}{2} h_2^2) = -g h_2 \partial_x(r h_1 + B(x)). \tag{2.4}$$

The above equations describes the mass and discharge equations for each layer of two-layer system, h_1 and h_2 being the heights of upper and lower layer respectively, while, u_1 and u_2 are velocities of the corresponding layers. Moreover, $q_i = h_i u_i$ for i = 1,2 are flow discharges and $B(x)$ is bottom topography. Furthermore, g is the gravity constant and r is the ratio of the densities $(r = \rho_1 / \rho_2 < 1)$. In vector notation, the above equations reads as,

$$\mathbf{W}_t + \mathbf{F}(\mathbf{W})_x = \mathbf{S}(\mathbf{W}), \tag{2.5}$$

where

$$\mathbf{W} = \begin{pmatrix} h_1 \\ q_1 \\ h_2 \\ q_2 \end{pmatrix}, \quad \mathbf{F} = \begin{pmatrix} q_1 \\ q_1 u_1 + \frac{g}{2} h_1^2 \\ q_2 \\ q_2 u_2 + \frac{g}{2} h_2^2 \end{pmatrix}, \quad \text{and} \quad \mathbf{S} = \begin{pmatrix} 0 \\ -g h_1 \partial_x(h_1 + B(x)) \\ 0 \\ -g h_2 \partial_x(r h_1 + B(x)) \end{pmatrix}. \tag{2.6}$$

Here, $\mathbf{W}$ is the vector of conserved variables, $\mathbf{F}$ represents the vector of fluxes and $\mathbf{S}$ is the vector of non-conservative source terms. The discharges of two-layers are coupled through non-conservative product terms. The system given in Eqs. (2.5) and (2.6) can be written in quasi-linear form as,

$$\mathbf{W}_t + \mathrm{A}(\mathbf{W})(\mathbf{W})_x = \mathbf{S}(\mathbf{W}), \tag{2.7}$$

where the Jacobian matrix $\mathrm{A}(\mathbf{W})$ is given by,

$$\mathrm{A}(\mathbf{W}) = \begin{pmatrix} 0 & 1 & 0 & 0 \\ g h_1 - u_1^2 & 2u_1 & g h_1 & 0 \\ 0 & 0 & 0 & 1 \\ r g h_2 & 0 & g h_2 - u_2^2 & 2u_2 \end{pmatrix}, \tag{2.8}$$

and

$$\mathbf{S}(\mathbf{W}) = \begin{pmatrix} 0 \\ -g h_1 B_x(x) \\ 0 \\ -g h_2 B_x(x) \end{pmatrix}. \tag{2.9}$$

Using the characteristic polynomial, the computed eigenvalues of the modified Jacobian satisfy,

$$(\lambda + u_1^2 - 2\lambda u_1 - gh_1)(\lambda + u_2^2 - 2\lambda u_2 - gh_2) = rgh_1h_2 \tag{2.10}$$

It can easily be observed that, the explicit form of eigenvalues cannot be evaluated. However, as long as $r \leq 1$, the system (2.1)-(2.5) will hyperbolic and the eigenvalues are turns to be real. There, we are concerned with flows in which the difference between u_1 and u_2 is small enough means $u_1 \approx u_2$ and $r \approx 1$ as in [7]. This yields to the first-order eigenvalues approximations as given by [5],

$$\lambda_{ext}^{\pm} = \frac{h_1u_1 + h_2u_2}{h} \pm \sqrt{gh}, \tag{2.11}$$

and

$$\lambda_{int}^{\pm} = \frac{h_1u_2 + h_2u_1}{h} \pm \sqrt{(1-r)\frac{gh_1h_2}{h}\left(1 - \frac{(u_2-u_1)^2}{(1-r)gh}\right)}. \tag{2.12}$$

The obtained approximation in [7, 10], is similar to that of ours with $h = h_1 + h_2$. From the eigenvalues, one can observe that the hyperbolicity of the system is directly linked with the values of $(u_1 - u_2)^2$. The system of Eqs. (2.1) to (2.5), as discussed above is conditionally hyperbolic and the system may lose the hyperbolicity if,

$$(u_1 - u_2)^2 > (1-r)gh. \tag{2.13}$$

One may note that this condition is not inflexible because the Eq. (2.13) is an approximation.

3. KFVS Scheme for Two-layer Shallow Water Equations

We split the derivation of KFVS scheme for the two-layer SWEs in three subsections. The derivation of this scheme is also available in [21, 22].

3.1 Introduction of Maxwellian distribution function

In this section the KFVS scheme is implemented to solve the two-layer SWEs given in (2.5) and (2.6). The movement of particles across the cell's interfaces is associated with the flow of conserved quantities. The local MDF [21] is utilized here for the distribution of moving particles in the x-direction. In normal direction $n \in \{x\}$ the MDF is stated as,

$$g_M(t,n,v_n) = h\left(\frac{\lambda_k}{\pi}\right)^{\frac{1}{2}} \exp\left[-\lambda_k(v_n - u_n)^2\right], \lambda_k = \frac{1}{gh}, \quad \text{for } k = 1,2. \tag{3.1}$$

where u_n is the average particle velocity, v_n is the individual particle velocity in n-direction and λ_k is normalization factor. Particles are categorized into two groups by using g_M defined in Eq. (3.1). Both the groups move in opposite directions with velocities ($u_n > 0$) and ($u_n < 0$) in right and left side of the interface. Let us first define the fluxes before splitting,

$$\langle v^0 \rangle_n = 1 = \int_{-\infty}^{\infty} \left(\frac{\lambda_k}{\pi}\right)^{\frac{1}{2}} e^{-\lambda_k(v_n-u_n)^2} dv, \tag{3.2}$$

$$\langle v^1 \rangle_n = u_n = \int_{-\infty}^{\infty} \left(\frac{\lambda_k}{\pi}\right)^{\frac{1}{2}} v_n e^{-\lambda_k(v_n-u_n)^2} dv. \tag{3.3}$$

In simplified form, we can define,

$$\langle v^0 \rangle_{-n} = \int_{-\infty}^{0} \left(\frac{\lambda_k}{\pi}\right)^{\frac{1}{2}} e^{-\lambda(v_n-u_n)^2} dv_n = \frac{1}{2}\text{erfc}(\sqrt{\lambda_k}u_n), \tag{3.4}$$

$$\langle v^0 \rangle_{-n} = \int_{-\infty}^{0} \left(\frac{\lambda_k}{\pi}\right)^{\frac{1}{2}} e^{-\lambda(v_n-u_n)^2} dv_n = \frac{1}{2}\text{erfc}(\sqrt{\lambda_k}u_n), \tag{3.5}$$

and

$$\langle v^1 \rangle_{+n} = \int_{0}^{\infty} \left(\frac{\lambda_k}{\pi}\right)^{\frac{1}{2}} v_n e^{-\lambda_k(v_n-u_n)^2} dv_n = u_n\langle v^0 \rangle_{+n} + \frac{1}{2}\frac{e^{-\lambda_k u_n^2}}{\sqrt{\pi\lambda_k}}, \tag{3.6}$$

$$\langle v^1 \rangle_{-n} = \int_{-\infty}^{0} \left(\frac{\lambda_k}{\pi}\right)^{\frac{1}{2}} v_n e^{-\lambda_k(v_n-u_n)^2} dv_n = u_n\langle v^0 \rangle_{-n} - \frac{1}{2}\frac{e^{-\lambda_k u_n^2}}{\sqrt{\pi\lambda_k}}. \tag{3.7}$$

3.2 Implementation of finite volume scheme

To implement any numerical algorithm, one has to divide the computational domain into N sub-domains. We define the cell $I_i = [x_{i+1/2}, x_{i-1/2}]$ for $i = 1,2,3....N$ and $\Delta x = x_{i+1/2} - x_{i-1/2}$. The cell center is denoted as $x_i = i\Delta x$, while the cell faces are defined as $x_{i\pm1/2} = x_i \pm \Delta x/2$. We proceed with the cell averaged initial data $\mathbf{W}_i^n$ for time t^n and calculate updated solution $\mathbf{W}_i^{n+1}$ at

next time level t^{n+1}. In light of the preceding definitions, the flux functions in (2.6) are splitted as,

$$\mathbf{F}(\mathbf{W}_i)=\begin{pmatrix} q_1 \\ q_1u_1+\dfrac{g}{2}h_1^2 \\ q_2 \\ q_2u_2+\dfrac{g}{2}h_2^2 \end{pmatrix}=\mathbf{F}^{+}+\mathbf{F}^{-}, \tag{3.8}$$

where

$$\mathbf{F}^{\pm}=\langle v^1\rangle_{\pm n}\begin{pmatrix} h_1 \\ h_1u_1 \\ h_2 \\ h_2u_2 \end{pmatrix}+\langle v^0\rangle_{\pm n}\begin{pmatrix} 0 \\ \dfrac{1}{2}gh_1^2 \\ 0 \\ \dfrac{1}{2}gh_2^2 \end{pmatrix}. \tag{3.9}$$

The fluxes in left and right direction of I_i are defined by,

$$\mathbf{F}_{i-\frac{1}{2}}=\mathbf{F}^{+}_{i-1}+\mathbf{F}^{-}_{i}, \quad \text{and} \quad \mathbf{F}_{i+\frac{1}{2}}=\mathbf{F}^{+}_{i}+\mathbf{F}^{-}_{i+1}, \tag{3.10}$$

Integrating Eq. (2.5) over the cell $I_i:=\left[x_{i-1/2},x_{i+1/2}\right]$ yields the semi-discrete scheme shown below,

$$\frac{d\mathbf{W}_i}{dt}=-\frac{\mathbf{F}_{i+\frac{1}{2}}-\mathbf{F}_{i-\frac{1}{2}}}{\Delta x}-\frac{\mathbf{S}_{i+\frac{1}{2}}-\mathbf{S}_{i-\frac{1}{2}}}{\Delta x}, \tag{3.11}$$

here, $\mathbf{W}_i$ is defined as,

$$\mathbf{W}_i:=\mathbf{W}_i(t)=\frac{1}{\Delta x}\int_{x_{i-\frac{1}{2}}}^{x_{i+\frac{1}{2}}}\mathbf{W}(t,x)dx \tag{3.12}$$

The modified Godunov-type methodology is utilized to discretize non-conservative terms in Eq. (2.5).

$$\mathbf{S}_{i+\frac{1}{2}}-\mathbf{S}_{i-\frac{1}{2}}=\begin{pmatrix} 0 \\ g(h_1)_i[(h_2)_{i+\frac{1}{2}}-(h_2)_{i-\frac{1}{2}}+B_{i+\frac{1}{2}}-B_{i-\frac{1}{2}}] \\ 0 \\ g(h_2)_i[r((h_1)_{i+\frac{1}{2}}-(h_1)_{i-\frac{1}{2}})+B_{i+\frac{1}{2}}-B_{i-\frac{1}{2}}] \end{pmatrix}. \tag{3.13}$$

where

$$(h_k)_{i-\frac{1}{2}}=(h_k)^{+}_{i-1}+(h_k)^{-}_{i} \quad \text{and} \quad (h_k)_{i+\frac{1}{2}}=(h_k)^{+}_{i}+(h_k)^{-}_{i+1} \quad \text{for} \quad k=1,2\,.$$

3.3 Extension to second-order scheme

The scheme (3.11) is first order accurate in space. In order to achieve higher order accuracy, the following initial reconstruction method is used for interpolation of the averaged cell variables. The slope vector $\mathbf{W}^{x}_{i}$, piecewise constant solution $\mathbf{W}_i$, and the extrapolated boundary values are use as in [21],

$$\mathbf{W}^{LX}_{i}=\mathbf{W}_i-\frac{1}{2}\mathbf{W}^{x}_{i}, \mathbf{W}^{RX}_{i}=\mathbf{W}_i+\frac{1}{2}\mathbf{W}^{x}_{i}. \tag{3.14}$$

$\mathbf{W}^{LX}_{i}$ and $\mathbf{W}^{RX}_{i}$ are the MUSCL reconstruction of $\mathbf{W}_i$,

$$\mathbf{W}^{x}_{i}=MM\left\{\theta\Delta\mathbf{W}_{i+\frac{1}{2}}, \quad \frac{1}{2}\left(\Delta\mathbf{W}_{i+\frac{1}{2}}+\Delta\mathbf{W}_{i-\frac{1}{2}}\right), \quad \theta\Delta\mathbf{W}_{i-\frac{1}{2}}\right\}, \tag{3.15}$$

where $1\le\theta\le 2$. The central differencing is defined as: $\Delta\mathbf{W}_{i+1/2}=\mathbf{W}_{i+1}-\mathbf{W}_i$. To handle the oscillations in the solution profile we use the following limiter [22],

$$MM\{x_1,x_2,x_3...\}=\begin{cases}\min_i\{x_i\} & \text{if } x_i<0 \quad \forall i, \\ \min_i\{x_i\} & \text{if } x_i>0 \quad \forall i, \\ 0 & \text{otherwise.}\end{cases} \tag{3.16}$$

Using the above procedure, the following high resolution scheme is obtained,

$$\frac{d\mathbf{W}_i}{dt}=-\frac{\mathbf{F}_{i+\frac{1}{2}}(\mathbf{W}^{LX}_{i+1},\mathbf{W}^{RX}_{i})-\mathbf{F}_{i-\frac{1}{2}}(\mathbf{W}^{LX}_{i},\mathbf{W}_{i-1}{}^{RX})}{\Delta x}-\frac{\mathbf{S}_{i+\frac{1}{2}}(\mathbf{W}^{LX}_{i+1},\mathbf{W}^{RX}_{i})-\mathbf{S}_{i-\frac{1}{2}}(\mathbf{W}^{LX}_{i},\mathbf{W}^{RX}_{i-1})}{\Delta x}. \tag{3.17}$$

where

$$\mathbf{F}_{i+\frac{1}{2}}(\mathbf{W}_{i+1}^{LX},\mathbf{W}_{i}^{RX})=\mathbf{F}_{i}^{+}(\mathbf{W}_{i}^{RX})+\mathbf{F}_{i+1}^{-}(\mathbf{W}_{i+1}^{RX}), \tag{3.18}$$

and

$$\mathbf{S}_{i+\frac{1}{2}}(\mathbf{W}_{i+1}^{LX},\mathbf{W}_{i}^{RX})=\mathbf{S}_{i}^{+}(\mathbf{W}_{i}^{RX})+\mathbf{S}_{i+1}^{-}(\mathbf{W}_{i+1}^{RX}). \tag{3.19}$$

A total variation diminishing RK method is applied to solve Eq. (3.17) to get second order accuracy of the suggested scheme. We take right side of Eq. (3.19) as $L(\mathbf{W})$. To update W, the following two stages are used [22],

$$\mathbf{W}^{(1)}=\mathbf{W}^{n}+\Delta tL(\mathbf{W}^{n}), \tag{3.20}$$

$$\mathbf{W}^{n+1}=\frac{1}{2}\left(\mathbf{W}^{n}+\mathbf{W}^{(1)}+\Delta tL(\mathbf{W}^{(1)})\right), \tag{3.21}$$

where $\Delta t=t^{n+1}-t^{n}$. Moreover,

$$\Delta t=\frac{\Delta x}{2\,|\,\mu_{k}\,|}.$$

with μ_{k} being the maximum eigenvalue.

4. Numerical Case Studies

In this section, several test problems are considered to analyze the performance of the proposed KFVS and CESE schemes. The outflow boundary conditions are used for problem 2-5.

Problem 1: Accuracy test problem.

This test case study is normally considered to find the accuracy order of a scheme see e.g. [30]. We also intend to calculate the order of our suggested scheme. The initial data are,

$$h_{1}=5+e^{\cos(2\pi x)},\quad h_{2}=5-e^{\cos(2\pi x)},\quad u_{1}(x,0)=u_{2}(x,0). \tag{4.1}$$

The bottom topography is $B(x)=sin^{2}(\pi x)$ with $x\in[0,1]$, $t=1.0$. Periodic boundary conditions are considered. Table 1 shows the experimental order of convergence (EOC) and L^{1}-errors in the solutions of KFVS and CESE schemes. We can observe from table 1 that our suggested KFVS scheme produces less errors as compared to the CESE scheme.

Problem 2: Steady state of rest

The motivation behind this example is a numerical demonstration of the capacity of our KFVS scheme to capture steady state of rest. The initial data representing stationary steady-state is,

$$(h_{1},q_{1},h_{2},q_{2})=\begin{cases}(0.59959,0,0.40152,0) & \text{if}\quad x\in[-0.6,-0.5],\\ (0.6,0,0.4,0) & \text{otherwise.}\end{cases} \tag{4.2}$$

The problem is studied with bottom topography $B(x)$ given as,

$$B(x)=\begin{cases}\frac{1}{4}[1+\cos(10\pi(x-0.5))] & \text{if}\quad x\in[-0.6,-0.5],\\ 0 & \text{otherwise.}\end{cases} \tag{4.3}$$

The value of $g=10$, density ratio r is 0.6 and our computational domain is [–1, 1]. The results are computed on two mesh sizes $\Delta x=1/100$, $\Delta x=1/200$ and the reference solution is obtained on $\Delta x=1/1000$. The results obtained by the KFVS and the CESE schemes are shown in Fig. 1. We can observe disturbance initially in the solutions of $h+B(x)$. The oscillation-free solution is obtained after some time.

Table 1. L^{1}-error comparison.

	h_1			u_2		
N	KFVS	CESE	ECO(KFVS)	KFVS	CESE	ECO(KFVS)
50	2.71×10^{-4}	3.41×10^{-4}	-	3.81×10^{-4}	4.7×10^{-4}	-
100	6.82×10^{-5}	9.58×10^{-5}	1.99	9.91×10^{-5}	1.20×10^{-4}	1.94
200	1.60×10^{-5}	2.34×10^{-5}	2.09	2.31×10^{-5}	3.42×10^{-5}	2.10
400	3.97×10^{-6}	6.04×10^{-6}	2.01	5.47×10^{-6}	9.11×10^{-6}	2.07
800	9.47×10^{-7}	1.60×10^{-6}	2.06	1.20×10^{-6}	2.25×10^{-6}	2.18
1600	2.21×10^{-7}	3.87×10^{-7}	2.09	2.76×10^{-7}	2.34×10^{-7}	2.12

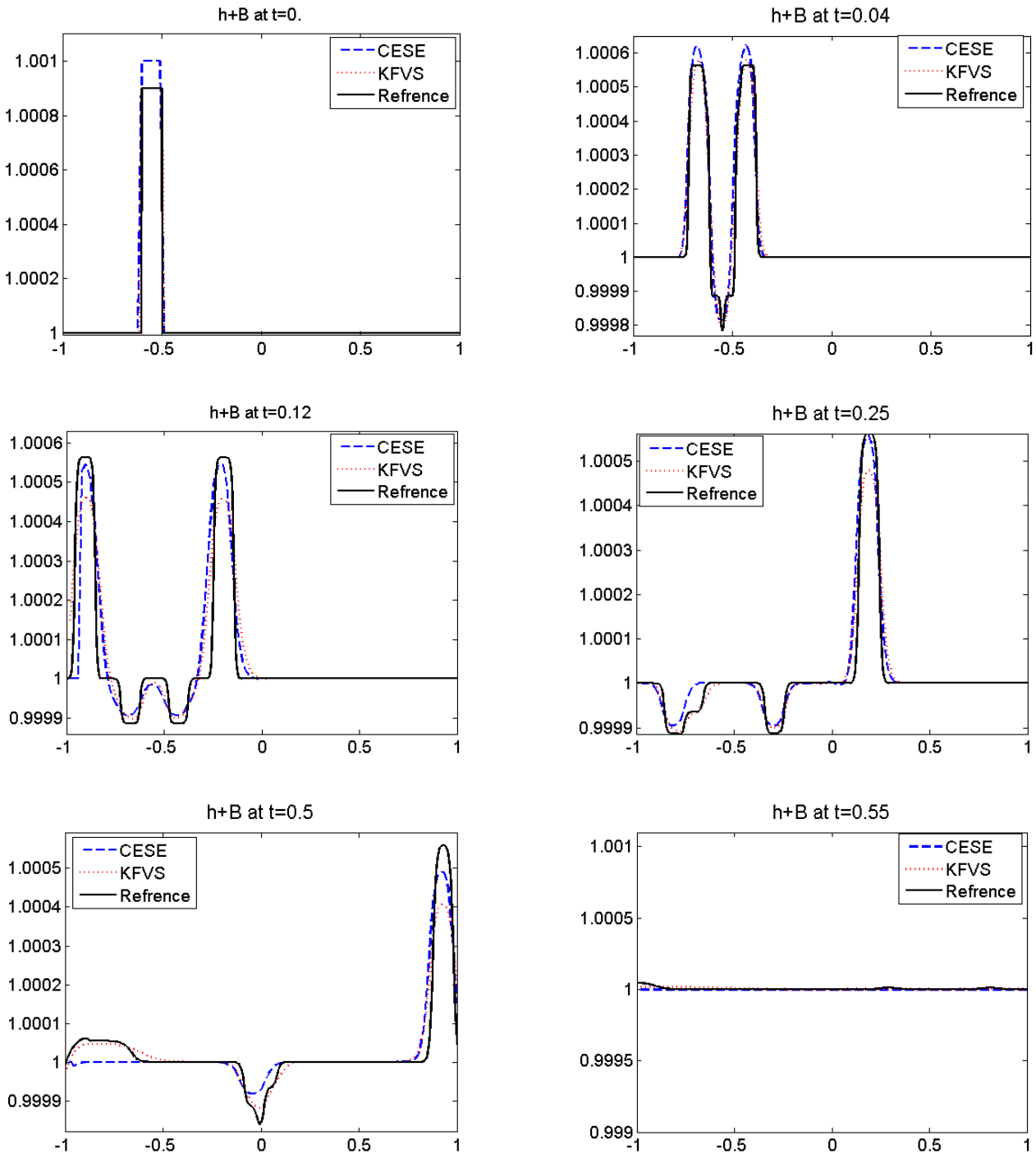

Fig. 1. Problem 2: Small perturbation of steady state: Free surface displacement $h + B(x)$ at different time steps as shown at $\Delta x = 1/100$ grids point on left side and $\Delta x = 1/200$ grids point on right.

Problem 3: Interface propagation I.

This test case study is used to check the capability of the KFVS scheme to propagate and capture discontinuities over time. Several authors frequently used this type of examples for validating their schemes for multi-layer flows [5, 12]. The initial data is given as,

$$(h_1, q_1, h_2, q_2) = \begin{cases} (0.50, 1.250, 0.50, 1.250) & \text{for } x < 0.3, \\ (0.45, 1.125, 0.55, 1.375) & \text{for } x > 0.3, \end{cases} \tag{4.4}$$

with flat bottom topography $B(x) = -1$. The constant of gravity $g = 10$ and the value of density ratio represented by r is 0.98. The computational domain for this problem is [0, 1]. The interface is taken at $x = 0.3$ initially. In this problem we take a smaller initial jump near the interface. The results are obtained at final simulation time $t = 0.1$ on two different mesh sizes, i.e. $\Delta x = 1/200$ and $1/800$. The reference solution is obtained on 10000 mesh cells.

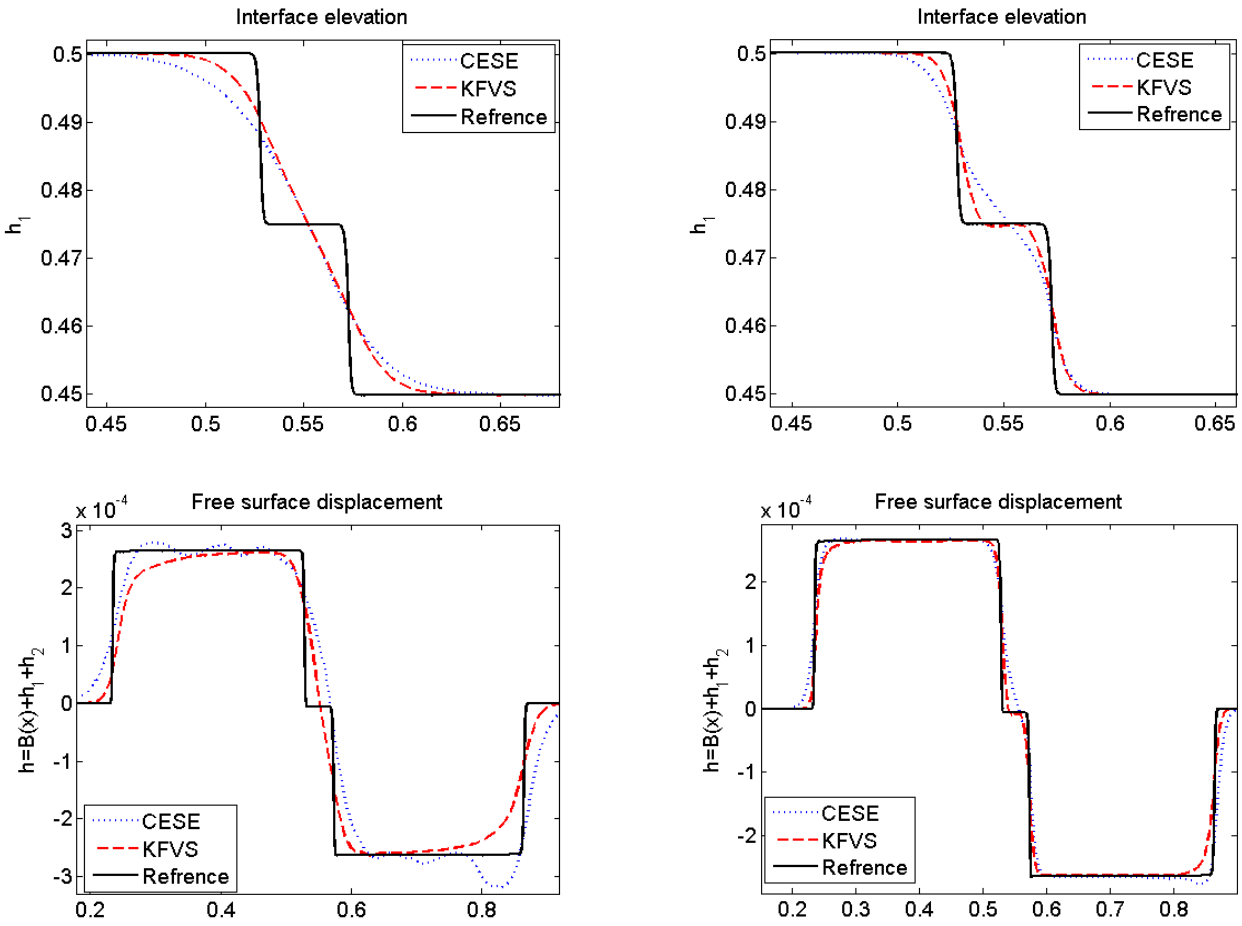

Fig. 2. Problem 3: Interface elevation on 200 grids point left and 800 grids point right.

The interface evolution of the fluid flow in the Fig. 2-3 shows that KFVS schemes guarantees better resolution as compared to that of CESE scheme. In Figure 2 (top left), the low resolution indicates that the interface stays sharp while propagating to the right and is diffusive due to the numerical viscosity. The results on refine mesh are displayed in (see Fig. 2(top right)).

The water surface $h_1 + h_2 + B(x)$ and upper layer velocity u_1 are plotted respectively in Figs. 2 and 3. The original sharp interface generates four waves that travel at four distinct distinctive speeds. We can clearly see that our proposed KFVS scheme produce good results after mesh refinement, there is no oscillation in free surface displacement while the results of Fig. 2, in [7], shows some oscillations even after refined mesh size up to $\Delta x = 1/800$ which practically shows the superiority of our scheme.

Problem 4: Interface propagation II.

This example is taken from [7, 10]. In this second problem of interface propagation, a much complicated case is considered at the interface with a comparatively large initial jump,

$$(h_1, q_1, h_2, q_2) = \begin{cases} (1.8, 0.0, 0.2, 0.0) & \text{for } x < 0, \\ (0.2, 0.0, 1.8, 0.0) & \text{for } x > 0, \end{cases} \tag{4.5}$$

with flat bottom function $B(x) = -2$ and same gravitational constant and density ratio is considered as in Problem 3. The results for free-water displacement h are obtained on a computational domain [–5, 5], whereas solution for h_2 is obtained from $x = 0$ to $x = 1$. This example is also solved using time splitting scheme which produce unphysical stationary shock [6]. We have computed the solution for h_2-component of the flow and free water surface at $t = 1$, using shock capturing KFVS scheme on two different mesh sizes, i.e. $\Delta x = 1/50$ and $1/100$. The reference solution computed with KFVS scheme is obtained on a bit refined grids with $\Delta x = 1/500$. The key feature of the proposed KFVS scheme is positivity preserving property, which can be seen in Fig. 4 (top).

Problem 5: Lock exchange flows.

This problem is also considered in [10]. Here, the two layers of water are at rest initially and separated by a membrane. The water with low density (lighter water) is on the left and that of high density (heavier water) is on the right. The data for the problem is given as under,

$$(h_1, q_1, h_2, q_2) = \begin{cases} (-B(x), 0.0, 0.0, 0.0) & \text{for } x < 0, \\ (0.0, 0.0, -B(x), 0.0) & \text{for } x > 0. \end{cases} \tag{4.6}$$

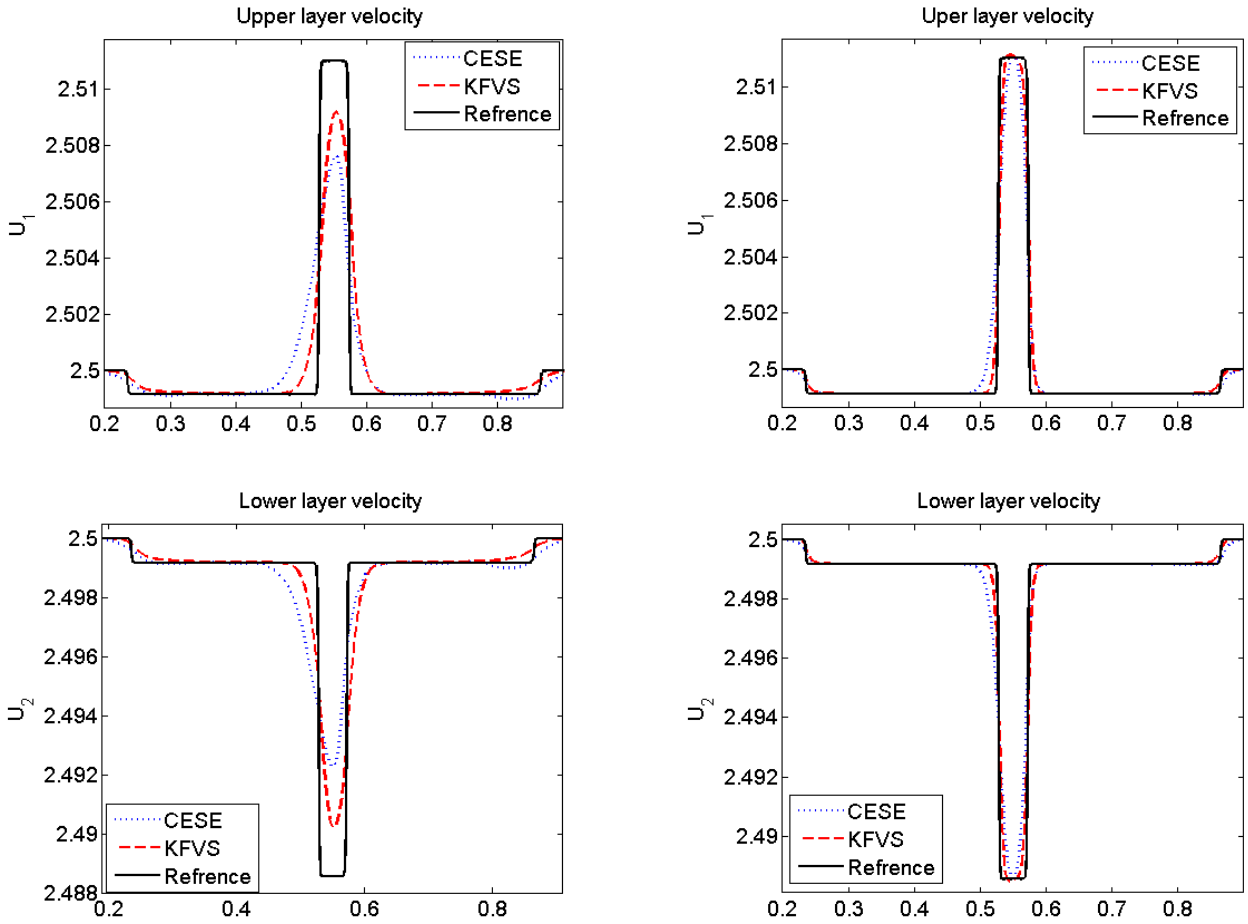

Fig. 3. Problem 3: Upper and lower layer velocities u_1 and u_2 on 200 grids point (left) and 800 grids point (right).

The Gaussian-shape $B(x)$ is given as,

$$B(x) = exp(-x^2) - 2. \tag{4.7}$$

The constant of gravity is $g = 9.81$, and however, $r = 0.98$. The computational domain is from $x = -3$ to $x = 3$, and at the ends of our interval the condition $q_1 = -q_2$, is imposed. The propagation of the heavier water is in the negative direction and vice versa. Our expectation from the solution is to converge to a non-stationary steady state. The results are given in Fig. 5.

Problem 6: Internal dam break.

The present problem is also discussed in [10], over a continuous bottom topography function. Because of the presence of hydraulic jump, the computation of steady-state problem is more difficult than that of previous one. The data for the said problem is given as,

$$(h_1, q_1, h_2, q_2) = \begin{cases} (1.95, 0.0, -1.95 - B, 0.0) & \text{for } x < 0, \\ (0.05, 0.0, -0.05 - B, 0.0) & \text{for } x > 0, \end{cases} \tag{4.8}$$

with continuous bottom topography function given by,

$$B(x) = 0.5\exp(-x^2) - 2.5. \tag{4.9}$$

Again the constant of gravity is same as in previous problem i.e. $g = 9.81$, and value of density ratio $r = 0.998$ is taken. The domain $[-5,5]$ is divided into $1/500$ grid points with imposing free boundary conditions at the ends. The results are depicted in Fig 6. We can clearly observe that KFVS is giving better results as compared to CESE scheme.

Problem 7: Dam break problem.

The data for this Riemann problem is,

$$(h_1, h_2, u_1, u_2)_l = (0.8, 0.2, 0, 0), \quad \text{if } x \le 0, \tag{4.10}$$

$$(h_1, h_2, u_1, u_2)_r = (1, 0, 0, 0), \quad \text{if } x > 0. \tag{4.11}$$

The interface is located at $x = 0$, with flat basal topography, i.e. $B(x) = \text{constant}$. For this problem, we have taken $h_2 = 0$ after $x > 0$. The results are depicted in Fig. 7. We can observe that there is no oscillation produced in the solution profiles obtained by KFVS and CESE schemes.

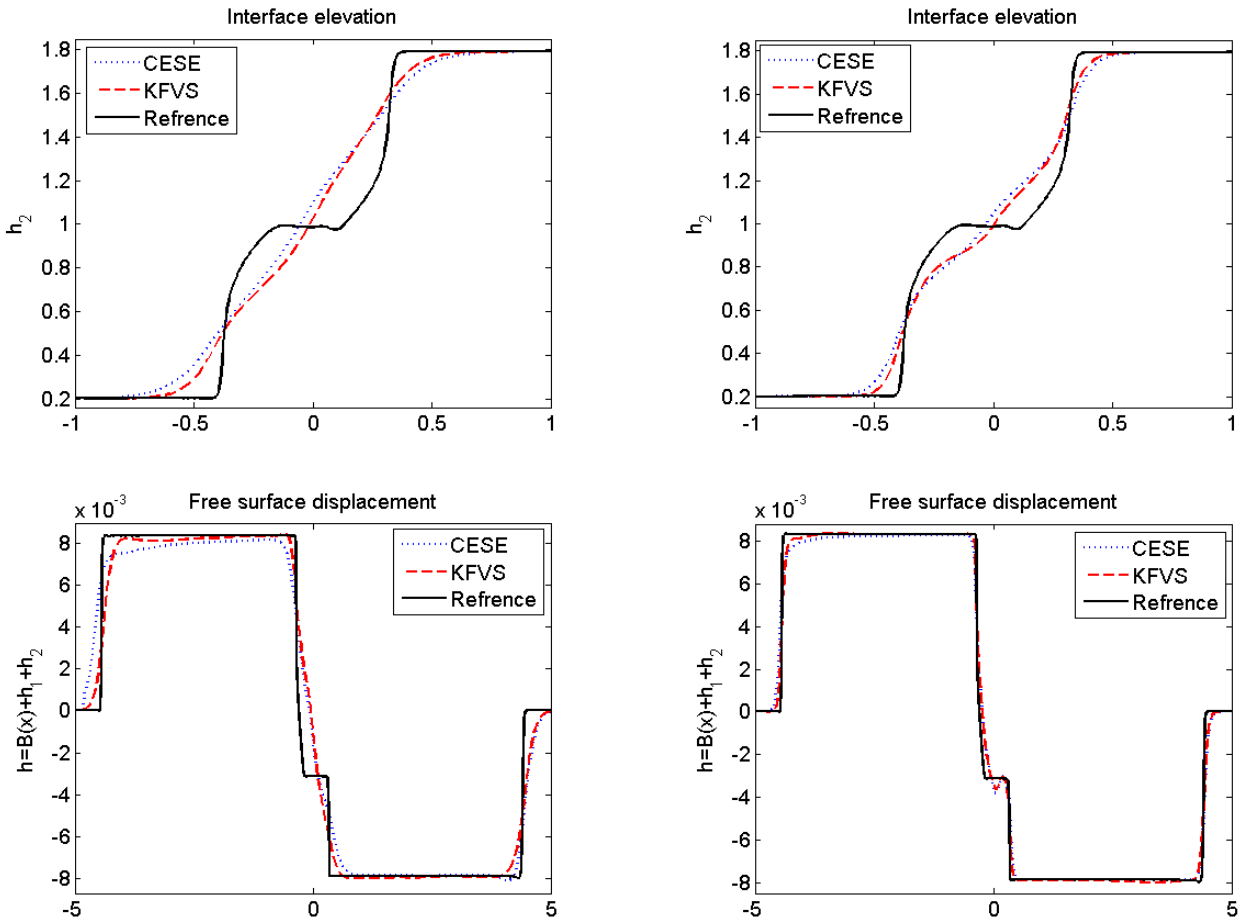

Fig. 4. Problem 4: Interface elevation h_2 (left) and free surface displacement $h_1 + h_2 + B(x)$ (right) on 50 and 100 grids.

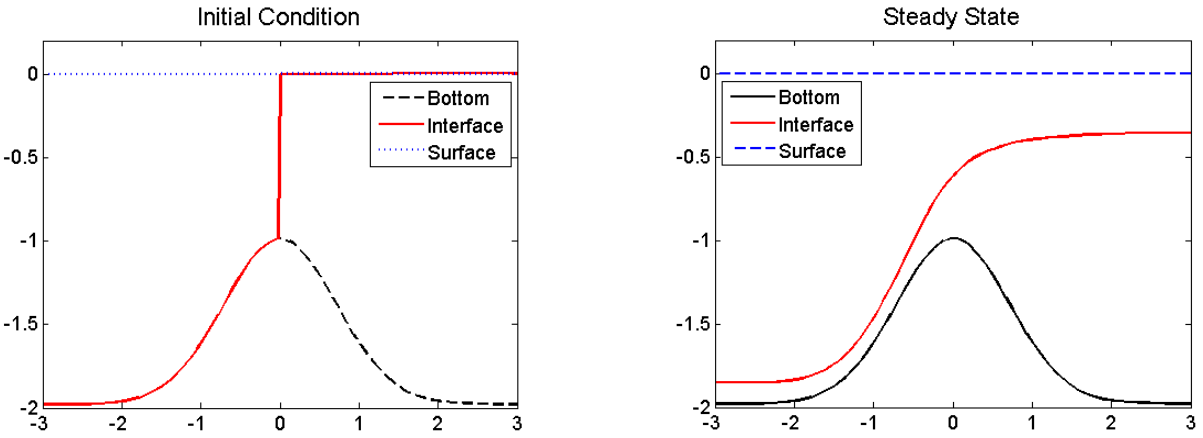

Fig. 5. Problem 5: Water surface ($h_1 + h_2 + B(x)$), interface ($h_2 + B(x)$) and $B(x)$.

5. Conclusion

In this work, two-layer SWEs were studied numerically. The KFVS scheme was suggested to study the model equations numerically. The model was conditionally hyperbolic and there was a possibility that system may lose hyperbolicity while solving it. The proposed scheme effectively handled this problem. The test cases revealed the performance of the suggested method to handle a wide number of flow conditions. The results were compared with those obtained from CESE scheme. The solutions by both the schemes were in good agreement with each other. However, the KFVS scheme provided better resolution of shocks. In addition, KFVS produced less L-1 error as compared to the CESE scheme.

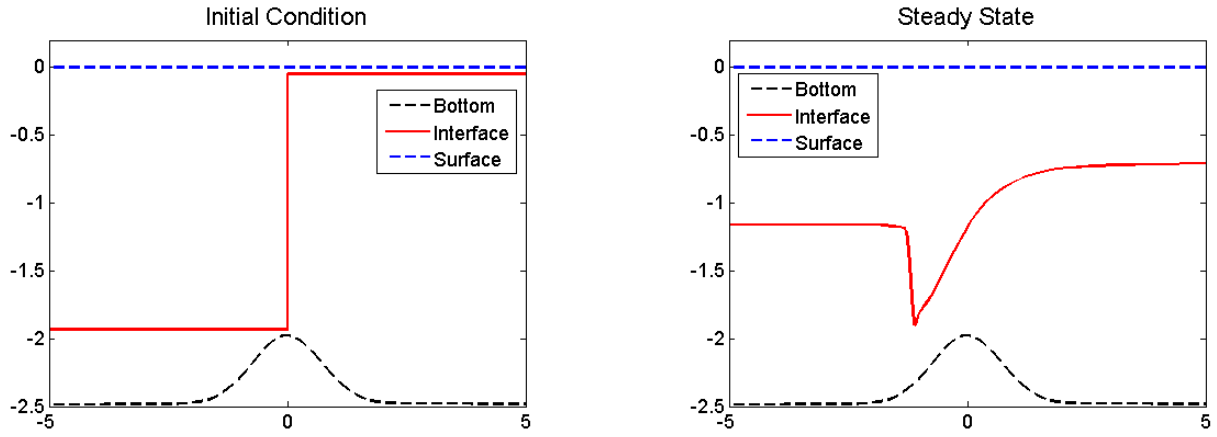

Fig. 6. Problem 6: Water surface ($h_1 + h_2 + B(x)$), interface ($h_2 + B(x)$) and $B(x)$.

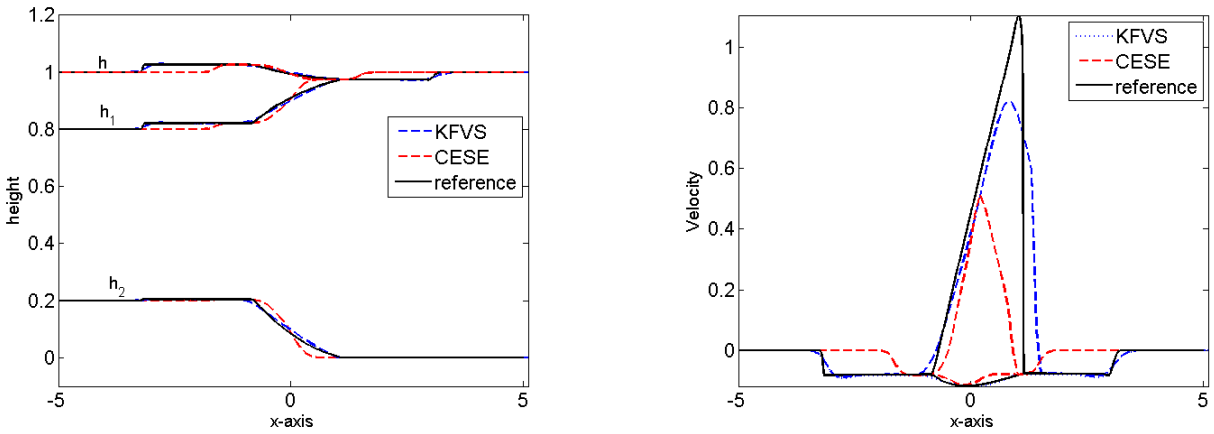

Fig. 7. Problem 7: Dam break problem. Results at t = 1.

Author Contributions

S. Zia initiated the project, and suggested the experiments; S. Ullah Khan worked on computer codes of test problems 2 and 4; Omar Rabbani worked on test problems 3-6 and also generated the table 1; M. Ahmed helped in computer codes, A. Rehman worked on writing the manuscript. All authors discussed the results, reviewed, and approved the final version of the manuscript.

Acknowledgments

Not Applicable

Conflict of Interest

The authors declared that they have no conflict of interest.

Funding

The authors received no financial support for the research, authorship, and publication of this article.

Data Availability Statements

All the data is provided in the manuscript.

References

[1] Castro, M. J., Garc´ıa-Rodr´ıguez, J. A., Gonz´alez-Vida, J. M., Mac´ıas, J., & Par´es, C., Improved FVM for two-layer shallow-water models: Application to the Strait of Gibraltar, *Advances in Engineering Software*, 38(6), 2007, 386-398.
[2] Ostapenko, V. V., Numerical simulation of wave flows caused by a shoreside landslide, *Journal of Applied Mechanics and Technical Physics*, 40(4), 1999, 647-654.
[3] Fern´andez-Nieto, E. D., Bouchut, F., Bresch, D., D´ıaz, M. C., & Mangeney, A., A new Savage-Hutter type model for submarine avalanches and generated tsunami, *Journal of Computational Physics*, 227(16), 2008, 7720-7754.
[4] Salmon, R., Numerical solution of the two-layer shallow water equations with bottom topography, *Journal of Marine Research*, 60(4), 2002, 605- 638.
[5] Abgrall, R., & Karni, S., Two-layer shallow water system: a relaxation approach, *SIAM Journal on Scientific Computing*, 31(3), 2009, 1603-1627.
[6] Bouchut, F., & de Luna, T. M., An entropy satisfying scheme for two-layer shallow water equations with uncoupled treatment, *ESAIM: Mathematical Modelling and Numerical Analysis*, 42(4), 2008, 683-698.
[7] Balb´as, J., & Karni, S., A non-oscillatory central scheme for one-dimensional two-layer shallow water flows along channels with varying width,

Journal of Scientific Computing, 55(3), 2013, 499-528.
[8] Castro-D´ıaz, M. J., Fern´andez-Nieto, E. D., Gonz´alez-Vida, J. M., & Par´es Madroal, C., Numerical treatment of the loss of hyperbolicity of the two-layer shallow-water system, *Journal of Scientific Computing*, 48(1), 2011, 16- 40.
[9] Ostapenko, V. V., Complete systems of conservation laws for two-layer shallow water models, *Journal of Applied Mechanics and Technical Physics*, 40(5), 1999, 796-804.
[10] Kurganov, A., & Petrova, G., Central-upwind schemes for two layer shallow water equations, *SIAM Journal on Scientific Computing*, 31(3), 2009, 1742-1773.
[11] D´az, M. C., Fern´andez-Nieto, E. D., Gonz´alez-Vida, J. M., Mangeney, A., & Par´es, C., A high-order finite volume method for nonconservative problems and its application to model submarine avalanches, *Integral Methods in Science and Engineering*, Vol. 2, 291-101, Birkhuser, Boston, 2010.
[12] Castro, M. J., Garc´ıa-Rodr´ıguez, J. A., Gonz´alez-Vida, J. M., Mac´ıas, J., Par´es, C., & Vzquez-Cendn, M. E., Numerical simulation of two-layer shallow water flows through channels with irregular geometry, *Journal of Computational Physics*, 195(1), 2004, 202-235.
[13] Pelanti, M., Bouchut, F., Mangeney, A., & Vilotte, J. P., Numerical modeling of two-phase gravitational granular flows with bottom topography, *In Hyperbolic problems: theory, numerics, applications*, Springer Berlin, Heidelberg, 2008.
[14] Pelanti, M., Bouchut, F., & Mangeney, A., A Roe-type scheme for two-phase shallow granular flows over variable topography, *ESAIM: Mathematical Modelling and Numerical Analysis*, 42(5), 2008, 851-885.
[15] Pelanti, M., Bouchut, F., & Mangeney, A., A Riemann solver for single phase and two-phase shallow flow models based on relaxation. Relations with Roe and VFRoe solvers, *Journal of Computational Physics*, 230(3), 2011, 515-550.
[16] Greenberg, J. M., & Leroux, A. Y., A well-balanced scheme for the numerical processing of source terms in hyperbolic equations, *SIAM Journal on Numerical Analysis*, 33(1), 1996, 1-16.
[17] Hubbard, M. E., & Garcia-Navarro, P., Flux difference splitting and the balancing of source terms and flux gradients, *Journal of Computational Physics*, 165(1), 2000, 89-125.
[18] Jin, S., A steady-state capturing method for hyperbolic systems with geometrical source terms, *ESAIM: Mathematical Modelling and Numerical Analysis*, 35(4), 2001, 631-645.
[19] Xu, K., Gas-kinetic theory-based flux splitting method for ideal magnetohydrodynamics, *Journal of Computational Physics*, 153(2), 1999, 334-352.
[20] Mandal, J. C., & Deshpande, S. M., Kinetic flux vector splitting for Euler equations, *Computers & Fluids*, 23(2), 1994, 447-478.
[21] Zia, S., & Qamar, S., A kinetic flux-vector splitting method for single-phase and two-phase shallow flows, *Computers & Mathematics with Applications*, 67(6), 2014, 1271-1288.
[22] Qamar, S., & Mudasser, S., A kinetic flux-vector splitting method for the shallow water magnetohydrodynamics, *Computer Physics Communications*, 181(6), 2010, 1109-1122.
[23] Deshpande, S. M., A Second-Order Accurate Kinetic-Theory-Based Method for Inviscid Compressible Flows, *NASA Langley Tech.*, 2613, 1986.
[24] Pullin, D. I., Direct simulation methods for compressible inviscid ideal gas flow, *Journal of Computational Physics*, 34, 1980, 231-244.
[25] Rietz, R. D., One-dimensional Compressible Gas Dynamics Calculations Using the Boltzmann Equation, *Journal of Computational Physics*, 42, 1981, 108.
[26] Perthame, B., Second-Order Boltzmann Schemes for Compressible Euler Equations in One and Two Space Dimensions, *SIAM Journal of Numerical Analysis*, 29(1), 1992, 1-19.
[27] Chang, S.C., The method of space time conservation element and solution element-A new approach for solving the Navier Stokes and Euler equations, *Journal of Computational Physics*, 119, 1995, 295-234.
[28] Chang, S.C., Wang, X.Y., & Chow, C.Y., New developments in the method of space-time conservation element and solution element-Applications to two-dimensional time-marching problems, *NASA TM 106758*, 1994.
[29] Chang, S.C., Wang, X. Y., & Chow, C. Y., The space-time conservation element and solution element method. A new high resolution and genuinely multidimensional paradigm for solving conservation laws, *Journal of Computational Physics*, 156, 1999, 89-136.
[30] Izem, N., Seaid, M., & Wakrim, M., A discontinuous Galerkin method for two-layer shallow water equations, *Mathematics and Computers in Simulation*, 120, 2016, 12-23.

ORCID iD

Saqib Zia https://orcid.org/0000-0002-4575-4987
Saeed Ullah Khan https://orcid.org/0000-0001-9468-0104
Omar Rabbani https://orcid.org/0000-0003-3344-7135
Asad Rehman https://orcid.org/0000-0003-1429-5543

How to cite this article: Zia S., Khan S.U., Rabbani O., Ahmed M., Rehman A. A Kinetic Flux-vector Splitting Scheme for Two-layer Shallow Flow Model, *J. Appl. Comput. Mech.*, 8(3), 2022, 1043–1053. https://doi.org/10.22055/jacm.2022.38275.3189